The International Journal of Advanced Manufacturing Technology (2019) 100:1839–1854
https://doi.org/10.1007/s00170-018-2821-0

ORIGINAL ARTICLE

Size-dependent responses of micro-end mill based on strain gradient elasticity theory

Yicong Du[1] · Qinghua Song[1,2] · Zhanqiang Liu[1,2] · Bing Wang[1] · Yi Wan[1,2]

Received: 3 May 2018 / Accepted: 1 October 2018 / Published online: 10 October 2018

Abstract

A significant size effect will occur on the tool part of micro-end mill due to its small diameter, which means the internal structure of the tool part material will affect the mechanical properties of the tool part. In view of this, a comprehensive method considering size effect is proposed in this paper to predict both the static and dynamic behaviors of micro-end mill more accurately. Based on the strain gradient elasticity theory (SGET) and Hamilton's principle, dynamic model of micro-end mill tool is presented, in which the Timoshenko beam model (TBM) considering the shear deformations and rotary inertia effects is employed. Based on the presented model, the static and dynamic behaviors of micro-end mill is obtained utilizing the finite element method (FEM). The influences of size effect on micro-end mill are investigated in detail by contrasting the static and dynamic behaviors of micro-end mill with different tool diameters and different length-to-diameter ratios, respectively. In order to verify the accuracy and efficiency of the presented method, an improved experiment is performed in this paper.

Keywords Micro-end mill · Size effect · Strain gradient elasticity theory · Static deflection · Dynamic response

Nomenclature

A	Area of cross-section
E	Young's modulus
I	Inertia moment of micro-end mill
$\mathbf{K}^e$	Element stiffness matrix
L	Total length of micro-end mill
L_t	Tool length of micro-end mill
M	Boundary classical moments
$\mathbf{M}^e$	Element mass matrix
M^h	Boundary higher-order moments
Q^h	Boundary higher-order force
T	Kinetic energy
U	Strain energy
V	Boundary shear force
W	Work done by external force
d_s	Shank diameter of micro-end mill
d_t	Tool diameter of micro-end mill
k	Bulk modulus
k_1, k_2, k_3, k_4, k_5, k_6	Coefficients
k_s	Shear coefficient
l_0, l_1, l_2	Material length-scale parameters
p_i, $\tau_{ijk}^{(1)}$, m_{ij}^s	Higher-order stresses tensors
q	Distributed lateral force
w	Transverse displacement
β	Shear angle
γ	Taper angle of micro-end mill
γ_i	Dilatation gradient tensor
ε_{ij}	Strain tensor
$\eta_{ijk}^{(1)}$	Deviatoric stretch gradient tensor
μ	Shear modulus
ν	Poisson's ratio
ρ	Density

✉ Qinghua Song
ssinghua@sdu.edu.cn

Yicong Du
du_yicong@163.com

Zhanqiang Liu
melius@sdu.edu.cn

[1] Key Laboratory of High Efficiency and Clean Mechanical Manufacture, Ministry of Education, School of Mechanical Engineering, Shandong University, Jinan, People's Republic of China

[2] National Demonstration Center for Experimental Mechanical Engineering Education, Shandong University, Jinan, People's Republic of China

σ_{ij}	Stress tensor
φ	Rotation angle
χ_{ij}^{s}	Symmetric part of the rotation gradient tensor

1 Introduction

Micro-parts with small size and high precision are increasingly playing a significant role in industries such as aerospace, biomedicine, electronics, information technology, and others [1, 2]. Micro-milling technology is one of the most versatile methods for manufacturing micro-parts due to its unique advantages of excellent three-dimensional machining capability, high machining accuracy, and variable processing materials [3, 4]. In order to achieve higher machining accuracy, the micro-end mill selected in micro-milling becomes smaller and smaller, and at present, the micro-end mill with tool diameter of 10 μm has been commercialized. Due to poor rigidity, micro-end mill has severe deflection and vibration than traditional end mill, which will affect the micro-milling force and machined surface quality [5, 6]. In order to satisfy the high-quality and high precision requirements of micro-parts, it is crucial to predict and control the vibration of the micro-end mill.

A number of researches have been done with regard to micro-end mill, and many micro-end mill models have been presented in recent years. Mustpha and Zhong [7] derived the governing equations of shank, taper, and flute of micro-end mill, respectively, and solved these sets of equations through spectral finite element method. Filiz [8] presented a three-dimensional model for micro-end mill considering the complex structure of fluted section and researched the effect of tool structure parameters on the natural frequencies based on the three-dimensional model. Yılmaz [9] presented an analytical model to determine the frequency response functions in tool point of micro-end mill using inverse stability analysis. Rodrigues [10] developed a tool deflection model based on the elasticity of materials theory and found that the effect of tool deflection will decrease the micro-milling force magnitude. Duncan et al. [11] presented an improved receptance coupling substructure analysis model for micro-end mill to predict the dynamic response of tool point. The research on the model and response of micro-end mill with tool diameter above 500 μm is quite mature. However, the research on micro-end mill with tool diameter less than 500 μm is rare.

In order to research the milling tool handily, the end mill is commonly assumed as a Euler-Bernoulli beam model (EBM). For example, Mijušković et al. [12] researched the tool deflection by building a static tool deflection analytical model based on Euler-Bernoulli beam model. Li et al. [13] researched the influence of geometrical features on tool static rigidity by assuming the end mill as Euler-Bernoulli beam. However, on account of the stubby nature of micro-end mill and high rotational speed in milling process, shear deformations and rotary inertia cannot be neglected and the Euler-Bernoulli beam model becomes less accurate. Therefore, the Timoshenko beam model (TBM) begins to be used to substitute Euler-Bernoulli beam model. Filiz et al. [14, 15] presented an analytical model of micro-end mill using Timoshenko beam model to research its dynamic characteristics, and the model was validated by experiment. Jun et al. [16] investigated the dynamic characteristics of micro-end mill using Timoshenko beam model by approximating the cross section of the fluted region to be circular.

The previous studies believe that the only difference between the micro-end mill and the macro-end mill is just the difference of size, so that all the studies research the micro-end mill based on the classical theory (CT). However, with the reduction of the tool diameter of micro-end mill, the internal structure of the material will affect the mechanical properties of the tool part of micro-end mill, and many new varieties such as kinetic and mechanic characteristics will occur, which is called size effect [17, 18]. Because of the lack of intrinsic length scale, the classical continuum theory fails to predict such size-dependent phenomenon [19]. During the past several years, some new high-order continuum theories have been developed and employed. Mindlin et al. [20] proposed the couple stress theory (CST) in which the function of strain energy considered strain tensor and rotation gradient tensor. For isotropic linear elastic material, the constitutive equation contains two material length-scale parameters in addition to the two elastic parameters, elastic modulus and Poisson's ratio. Due to the difficulties in determining the material length-scale parameters, Yang et al. [21] modified the couple stress theory in which a new additional equilibrium condition, moment of couple, based on the classical couple stress theory was introduced to govern the behavior of higher-order stresses and the equilibrium of force couple. In the modified couple stress theory (MCST), only one material length-scale parameter is contained in the constitutive equation. Although the couple stress theory contains material length-scale parameters describing the size effect, other tensors like strain gradient tensor are neglected. In order to perfect the high-order continuum theory, Mindlin et al. [22] proposed a strain gradient elasticity theory (SGET) in which the strain tensor, rotation gradient tensor, and stretch gradient tensor were considered in the function of strain energy. And the material length-scale parameters in strain gradient elasticity theory are three times more than the classical couple stress theory. Based on the strain gradient elasticity theory, Lam et al. [23] introduced a new equilibrium condition, moment of couple, to govern the behavior of higher-order stresses. In this theory, the strain energy is associated with the strain tensor, rotation gradient tensor, stretch gradient tensor, and dilatation gradient tensor, and the constitutive equation only contains three length-scale parameters. In

micro-milling process, the micro-end mill is assumed to be flexible relative to the rigid workpiece in most cases due to the size of the workpiece being usually larger than that of the micro-end mill [24]. As a consequence, the vibration amplitudes of micro-end mill are regarded as dominant factors affecting the surface roughness [25]. The research on the deflection and response of micro-end mill under the influence of size effect is crucial to improving the machined surface quality.

This paper presents a comprehensive method to research the static and dynamic problems of micro-end mill and study the influences of size effect on static deflection and vibration of micro-end mill. To begin with, the dynamic model (governing equations and boundary conditions) of micro-end mill is derived based on SGET and Hamilton's principle. Considering the shear deformations and rotary inertia effects, TBM is used in the derivation. Then the static deflection, modal characteristic, and dynamic response are obtained based on the finite element method. Meanwhile, the experiments are conducted to verify the accuracy and efficiency of the presented method. The conclusions are given in the end.

2 Model of micro-end mill

In general, the structure of micro-end mill can be divided into three parts, namely, shank, taper, and tool. As shown in Fig. 1, the geometric parameters of micro-end mill include total length (L), shank diameter (d_s), taper angle (γ), tool diameter (d_t), and tool length (L_t). Due to the existence of micro-flute in tool part, it is difficult to establish the dynamic model of the tool part of micro-end mill directly. Based on the equivalent method, the tool part is assumed to be a uniform beam which diameter is reduced to 68% [26].

In order to consider the size effect in micro-end mill model, the SGET is used to replace the CT. In strain gradient elastic theory, the strain energy of micro-end mill is associated with the dilatation gradient tensor (γ_i), the deviatoric stretch gradient tensor ($\eta_{ijk}^{(1)}$), the symmetric part of the rotation gradient tensor (χ_{ij}^{s}), and the higher-order stresses (p_i, $\tau_{ijk}^{(1)}$, and m_{ij}^{s}) besides the strain tensor (ε_{ij}) and the classical stress tensor (σ_{ij}) [23].

$$U = \iiint_{\Omega} \left(\sigma_{ij}\varepsilon_{ij} + p_i\gamma_i + \tau_{ijk}^{(1)}\eta_{ijk}^{(1)} + m_{ij}^{s}\chi_{ij}^{s} \right) \mathrm{d}V \tag{1}$$

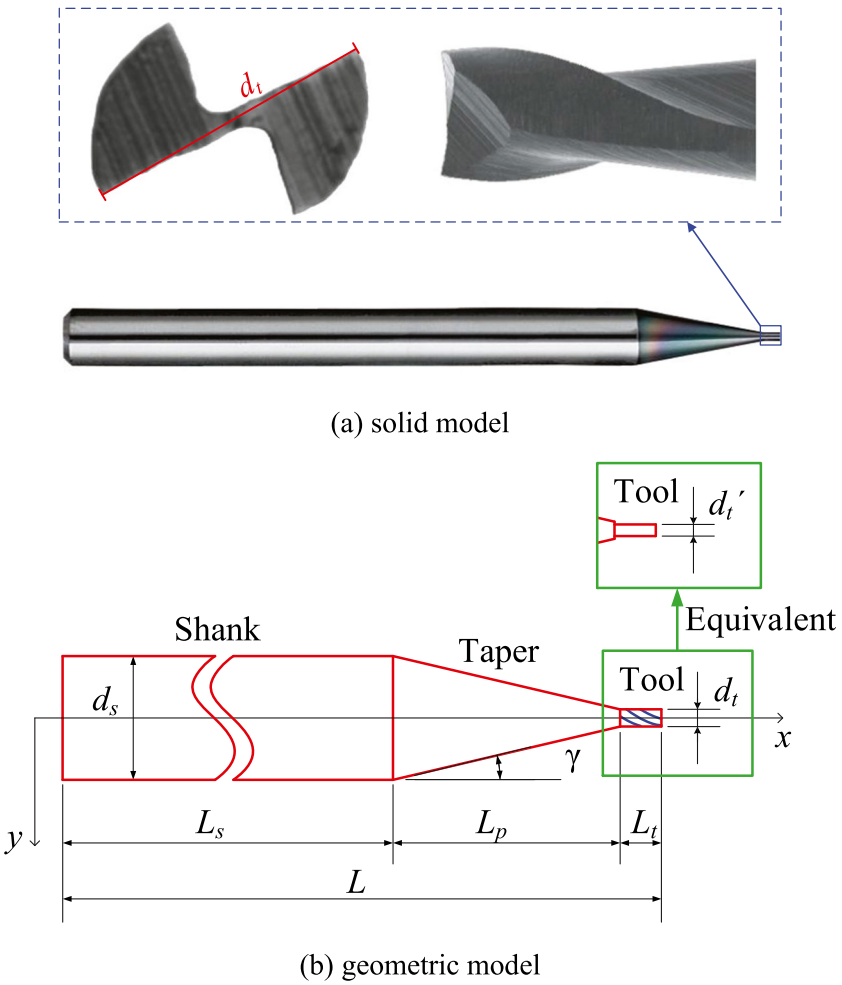

Fig. 1 Model of micro-end mill

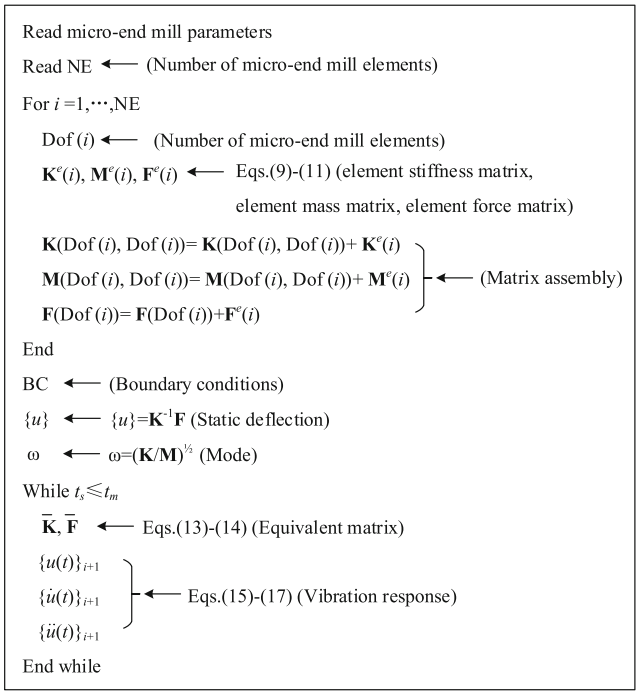

Fig. 2 Pseudocode of the proposed method

where the expression of ε_{ij}, γ_i, $\eta_{ijk}^{(1)}$, χ_{ij}^{s}, σ_{ij}, p_i, $\tau_{ijk}^{(1)}$, and m_{ij}^{s} are given in Appendix 1.

Based on the TBM considering the shear deformations and rotary inertia effects, the strain energy U of the micro-end mill can be determined. The detailed derivation process is shown in Appendix 2.

$$U=\frac{1}{2}\int_0^L\left[\begin{array}{l}(k_1+k_3)\varphi''^2+\left(I(x)\left(k+\frac{4}{3}\mu\right)+k_2\right)\varphi'^2\\+k_4\left(-w''+2\varphi'\right)^2+k_5\left(w''+\varphi'\right)^2+k_6\left(w'-\varphi\right)^2\end{array}\right]\mathrm{d}x \quad (2)$$

where,

$$k_1=2\mu l_0^2 I, k_2=2\mu A l_0^2, k_3=\frac{4}{5}\mu l_1^2 I, k_4=\frac{8}{15}\mu A l_1^2, k_5=\frac{1}{4}\mu A l_2^2, k_6=k_s\mu A \quad (3)$$

here, l_0, l_1, and l_2 are the material length-scale parameters which associated with size effect, k_s is the shear coefficient, A is the area of cross-section, and I is the inertia moment of micro-end mill. It should be noted that A and I are functions of length (x).

The kinetic energy can be given by [27].

$$T=\frac{1}{2}\int_0^L\left(\rho I\dot{\varphi}^2+\rho A\dot{w}^2\right)\mathrm{d}x \quad (4)$$

Additionally, the work done by distributed lateral force (q) along the x-axis, the boundary shear force (V), the boundary higher-order force (Q^{h}), the boundary classical moments (M), and the boundary higher-order moments (M^{h}) can be expressed as [28].

$$\delta W=\int_0^L q\delta w\mathrm{d}x+V\delta w\big|_0^L+Q^{\mathrm{h}}\delta\varphi\big|_0^L+M\delta w'\big|_0^L+M^{\mathrm{h}}\delta\varphi'\big|_0^L \quad (5)$$

According to Hamilton's principle [29], the governing equations of micro-end mill are derived as follows:

$$\begin{aligned}&(k_4+k_5)w^{(4)}+(-2k_4+k_5)\varphi'''-k_6\left(w''-\varphi'\right)+\rho A\ddot{w}=q\\&(k_1+k_3)\varphi^{(4)}-(-2k_4+k_5)w'''-(EI+k_2+4k_4+k_5)\varphi''-k_6\left(w'-\varphi\right)\\&\quad+\rho I\ddot{\varphi}=0\end{aligned} \quad (6)$$

From Eq. (6), it can be found that the micro-end mill model derived based on the SGET contains three material length-scale parameters (l_0, l_1, and l_2) that can reflect the size effect. It should be noted that the governing equations will degenerate to those derived based on the MCST when the two material length-scale parameters l_0 and l_1 are equal to zero. Further, the governing equations will degenerate to those derived based on the CT when the other material length-scale parameter l_2 is also equal to zero. Furthermore, when the shear deformations are neglected, the governing equations will degenerate to those based on the EBM.

In order to solve the governing equations of micro-end mill, the finite element method (FEM) is utilized. Now, a two-node Timoshenko beam element is assumed and two degrees of freedom (lateral deflection and rotation angle of cross-section) are assigned to each node. According to weighted-residual method, the final weak form of Eq. (6) over an element (x_{a}, x_{b}) can be expressed as

$$\begin{aligned}0=&\int_{x_{\mathrm{a}}}^{x_{\mathrm{b}}}\left[\begin{array}{l}(k_4+k_5)\frac{\mathrm{d}^2v_1}{\mathrm{d}x^2}\frac{\mathrm{d}^2w}{\mathrm{d}x^2}+(-2k_4+k_5)\frac{\mathrm{d}^2v_1}{\mathrm{d}x^2}\frac{\mathrm{d}\varphi}{\mathrm{d}x}\\+k_6\frac{\mathrm{d}v_1}{\mathrm{d}x}\frac{\mathrm{d}w}{\mathrm{d}x}-k_6\frac{\mathrm{d}v_1}{\mathrm{d}x}\varphi+v_1\rho A\frac{\mathrm{d}^2w}{\mathrm{d}t^2}-v_1q\end{array}\right]\mathrm{d}x\\&-v_1'(x_{\mathrm{a}})Q_1-v_1(x_{\mathrm{a}})Q_3-v_1'(x_{\mathrm{b}})Q_5-v_1(x_{\mathrm{b}})Q_7\\0=&\int_{x_{\mathrm{a}}}^{x_{\mathrm{b}}}\left[\begin{array}{l}(k_1+k_3)\frac{\mathrm{d}^2v_2}{\mathrm{d}x^2}\frac{\mathrm{d}^2\varphi}{\mathrm{d}x^2}+(-2k_4+k_5)\frac{\mathrm{d}v_2}{\mathrm{d}x}\frac{\mathrm{d}^2w}{\mathrm{d}x^2}+v_2\rho I\frac{\mathrm{d}^2\varphi}{\mathrm{d}t^2}\\+(EI+k_2+4k_4+k_5)\frac{\mathrm{d}v_2}{\mathrm{d}x}\frac{\mathrm{d}\varphi}{\mathrm{d}x}-k_6v_2\left(\frac{\mathrm{d}w}{\mathrm{d}x}-\varphi\right)\end{array}\right]\mathrm{d}x\\&-v_2(x_{\mathrm{a}})Q_2-v_2'(x_{\mathrm{a}})Q_4-v_2(x_{\mathrm{b}})Q_6-v_2'(x_{\mathrm{b}})Q_8\end{aligned} \quad (7)$$

where Q_i (i = 1,2,… ,8) is shown in Appendix 3.

Now, assuming that w and φ is interpolated by the following forms [30].

$$w(x,t_{\mathrm{s}})=\sum_{j=1}^{m}w_j^{\mathrm{e}}(t_{\mathrm{s}})\psi_j^{(1)}(x),\varphi(x,t_{\mathrm{s}})=\sum_{j=1}^{n}\varphi_j^{\mathrm{e}}(t_{\mathrm{s}})\psi_j^{(2)}(x) \quad (8)$$

and substituting $v_1=\psi_i^{(1)}(x)$ and $v_2=\psi_i^{(2)}(x)$ and Eq. (8) into Eq. (7), the element stiffness matrix $\mathbf{K}^e$ and element mass matrix $\mathbf{M}^e$ are obtained, and they are shown as follows.

Different with the classical theory, the element stiffness matrix is not only related to stress tensor but also to the dilatation gradient tensor, the deviatoric stretch gradient tensor, and the symmetric part of the rotation gradient tensor. When the size effect is neglected, $\mathbf{K}^{\mathrm{d}}$, $\mathbf{K}^{\mathrm{s}}$, and $\mathbf{K}^{\mathrm{r}}$ in Eq. (9) are equal to zero and the stiffness of micro-end mill is the same with the stiffness derived based on the classical theory. As a result, the stiffness of micro-end mill will increase when size effect is considered.

$$\mathbf{K}^{e}=\mathbf{K}^{\mathrm{c}}+\mathbf{K}^{\mathrm{d}}+\mathbf{K}^{\mathrm{s}}+\mathbf{K}^{\mathrm{r}}=\begin{bmatrix}\mathbf{K}^{\mathrm{c}11} & \mathbf{K}^{\mathrm{c}12}\\ \mathbf{K}^{\mathrm{c}21} & \mathbf{K}^{\mathrm{c}22}\end{bmatrix}+\begin{bmatrix}\mathbf{K}^{\mathrm{d}11} & \mathbf{K}^{\mathrm{d}12}\\ \mathbf{K}^{\mathrm{d}21} & \mathbf{K}^{\mathrm{d}22}\end{bmatrix}+\begin{bmatrix}\mathbf{K}^{\mathrm{s}11} & \mathbf{K}^{\mathrm{s}12}\\ \mathbf{K}^{\mathrm{s}21} & \mathbf{K}^{\mathrm{s}22}\end{bmatrix}+\begin{bmatrix}\mathbf{K}^{\mathrm{r}11} & \mathbf{K}^{\mathrm{r}12}\\ \mathbf{K}^{\mathrm{r}21} & \mathbf{K}^{\mathrm{r}22}\end{bmatrix} \tag{9}$$

$$\mathbf{M}^{e}=\begin{bmatrix}\mathbf{M}^{11} & \mathbf{M}^{12}\\ \mathbf{M}^{21} & \mathbf{M}^{22}\end{bmatrix}\quad \mathbf{F}^{e}=\begin{bmatrix}\mathbf{F}_1\\ \mathbf{F}_2\end{bmatrix} \tag{10}$$

where,

$$K_{ij}^{\mathrm{c}11}=\int_{x_{\mathrm{a}}}^{x_{\mathrm{b}}}k_6\frac{\mathrm{d}\psi_i^{(1)}}{\mathrm{d}x}\frac{\mathrm{d}\psi_j^{(1)}}{\mathrm{d}x}\mathrm{d}x,$$

$$K_{ij}^{\mathrm{c}22}=\int_{x_{\mathrm{a}}}^{x_{\mathrm{b}}}\left(EI\frac{\mathrm{d}\psi_i^{(2)}}{\mathrm{d}x}\frac{\mathrm{d}\psi_j^{(2)}}{\mathrm{d}x}+k_6\psi_i^{(2)}\psi_j^{(2)}\right)\mathrm{d}x$$

$$K_{ij}^{\mathrm{c}12}=\int_{x_{\mathrm{a}}}^{x_{\mathrm{b}}}\left(-k_6\frac{\mathrm{d}\psi_i^{(1)}}{\mathrm{d}x}\psi_j^{(2)}\right)\mathrm{d}x=K_{ij}^{\mathrm{c}21}$$

$$K_{ij}^{\mathrm{d}22}=\int_{x_{\mathrm{a}}}^{x_{\mathrm{b}}}\left(k_1\frac{\mathrm{d}^2\psi_i^{(2)}}{\mathrm{d}x^2}\frac{\mathrm{d}^2\psi_j^{(2)}}{\mathrm{d}x^2}+k_2\frac{\mathrm{d}\psi_i^{(2)}}{\mathrm{d}x}\frac{\mathrm{d}\psi_j^{(2)}}{\mathrm{d}x}\right)\mathrm{d}x$$

$$K_{ij}^{\mathrm{s}11}=\int_{x_{\mathrm{a}}}^{x_{\mathrm{b}}}k_4\frac{\mathrm{d}^2\psi_i^{(1)}}{\mathrm{d}x^2}\frac{\mathrm{d}^2\psi_j^{(1)}}{\mathrm{d}x^2}\mathrm{d}x,$$

$$K_{ij}^{\mathrm{s}22}=\int_{x_{\mathrm{a}}}^{x_{\mathrm{b}}}\left(k_3\frac{\mathrm{d}^2\psi_i^{(2)}}{\mathrm{d}x^2}\frac{\mathrm{d}^2\psi_j^{(2)}}{\mathrm{d}x^2}+4k_4\frac{\mathrm{d}\psi_i^{(2)}}{\mathrm{d}x}\frac{\mathrm{d}\psi_j^{(2)}}{\mathrm{d}x}\right)\mathrm{d}x$$

$$K_{ij}^{\mathrm{s}12}=\int_{x_{\mathrm{a}}}^{x_{\mathrm{b}}}\left((-2k_4)\frac{\mathrm{d}^2\psi_i^{(1)}}{\mathrm{d}x^2}\frac{\mathrm{d}\psi_j^{(2)}}{\mathrm{d}x}\right)\mathrm{d}x=K_{ij}^{\mathrm{s}21}$$

$$K_{ij}^{\mathrm{r}11}=\int_{x_{\mathrm{a}}}^{x_{\mathrm{b}}}k_5\frac{\mathrm{d}^2\psi_i^{(1)}}{\mathrm{d}x^2}\frac{\mathrm{d}^2\psi_j^{(1)}}{\mathrm{d}x^2}\mathrm{d}x,\ K_{ij}^{\mathrm{r}22}=\int_{x_{\mathrm{a}}}^{x_{\mathrm{b}}}\left(k_5\frac{\mathrm{d}\psi_i^{(2)}}{\mathrm{d}x}\frac{\mathrm{d}\psi_j^{(2)}}{\mathrm{d}x}\right)\mathrm{d}x$$

$$K_{ij}^{\mathrm{r}12}=\int_{x_{\mathrm{a}}}^{x_{\mathrm{b}}}k_5\frac{\mathrm{d}^2\psi_i^{(1)}}{\mathrm{d}x^2}\frac{\mathrm{d}\psi_j^{(2)}}{\mathrm{d}x}\mathrm{d}x=K_{ij}^{\mathrm{r}21}$$

$$M_{ij}^{11}=\int_{x_{\mathrm{a}}}^{x_{\mathrm{b}}}\left(\rho A\psi_i^{(1)}\psi_j^{(1)}\right)\mathrm{d}x,\ M_{ij}^{22}=\int_{x_{\mathrm{a}}}^{x_{\mathrm{b}}}\left(\rho I\psi_i^{(2)}\psi_j^{(2)}\right)\mathrm{d}x$$

$$F_i^1=\int_{x_{\mathrm{a}}}^{x_{\mathrm{b}}}q\psi_i^{(1)}\mathrm{d}x+Q_{2i-1},\ F_i^2=Q_{2i} \tag{11}$$

In order to overcome the shear-locking phenomenon, the Lagrange interpolation functions of $\psi_i^{(1)}$ and $\psi_i^{(2)}$ are selected as cubic polynomial and quadratic polynomial, respectively. Then the stiffness matrix and mass matrix of each unit are assembled to obtain the overall stiffness matrix and mass matrix. Since most finite element software is based on traditional continuum theory, it cannot be used to solve the size-dependent static and dynamic behaviors of micro-end mill. In this paper, the size-dependent static and dynamic behaviors of micro-end mill are obtained with the help of MATLAB software. The number of beam element in the shank part, taper part, and tool part is 500, 500, and 200, respectively, and the pseudocode of the proposed method is shown in Fig. 2.

3 Result analysis and discussion

3.1 Static deflection of micro-end mill

In micro-milling process, the shank of micro-end mill is fixed on the spindle of micro-milling machine while the tool part is free. Hence, the micro-end-mil is assumed as a cantilever Timoshenko beam. In order to study simply, the micro-milling force is equivalent to a concentrated constant force acting on the tool tip to research the deflection of micro-end mill in some cases. Therefore, the displacement of the micro-end mill is only a function of the length (x), independent of the time (t). Under the action of micro-milling force ($\boldsymbol{F}$), the static deflection of micro-end mill can be obtained through $\{u\}=\boldsymbol{K}^{-1}\boldsymbol{F}$.

In order to reveal the static deflection characteristics of micro-end mill, some numerical results are obtained and shown in Figs. 3 and 4 and Table 2. The geometric properties of micro-end mill selected in this section are shown in Table 1. And the material of micro-end mill is tungsten carbide of which density (ρ) = 14,900 kg/m^3, Young's modulus (E) = 630 GPa, Poisson's ratio (v) = 0.22, and shear coefficient (k_{s}) = 0.9. At present, the material length-scale parameters of many metals have been evaluated by experiment or derivation. Voyiadjis et al. [31] obtained the value of material length-scale parameters for cold-rolled 1018 steel and oxygen-free high-conductivity copper which were 13 and 1.5 μm, respectively, based on experimental observations. Song et al. [32] obtained the material length-scale parameters of face-centered cubic metals (Cu, Al, Ni, Ag, Au, Pt, and Pd) that ranged from 0.5 to 3 μm. However, the value of material length-scale parameters for tungsten carbide has not been reported. Without loss of generality, assume the material length-scale parameter $l_0=l_1=l_2=10$ μm for tungsten carbide here.

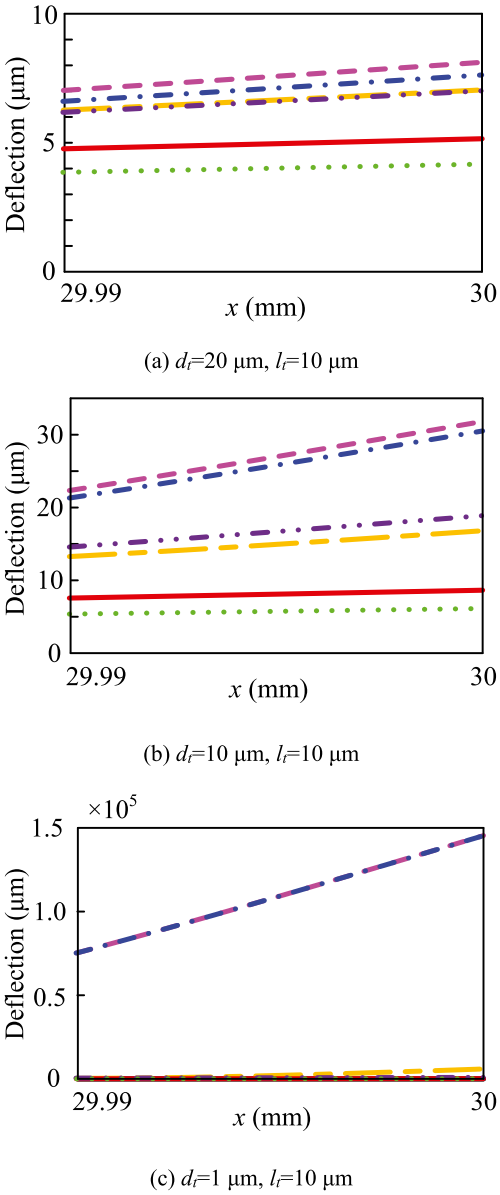

Fig. 3 Deflections of micro-end mills with different geometries

Since the micro-milling force is about 0.5 N in micro-milling process [24], in order to match the actual situation, the concentrated constant force (F) = 0.5 N is selected.

Figure 3 shows the static deflection results of micro-end mill calculated based on the SGET, the MCST, and the CT, respectively. The horizontal axis in Fig. 3 means the length coordinate value of micro-end mill, and the selected Cartesian coordinate system is shown in Fig. 1b. In Fig. 3, solid line, long dashed line, and dashed line represent the deflections calculated based on SGET, MCST, and CT when the micro-end mill is taken to be a TBM, respectively. Meanwhile, dotted line, double dashed-dotted line, and dashed-dotted line represent the deflections calculated based on SGET, MCST, and CT when the micro-end mill is taken to be a EBM, respectively. It can be obviously found that the deflection of micro-end mill mainly occurred in the tool part because of the small tool diameter. For instance, the deflection of the tool part contributes 90% to the total deflection based on the new model when the tool diameter equals to 1 μm and tool length equals to 10 μm. And with the increase of tool diameter, the deflection of tool part decreases. This phenomenon is the same as the research proceeded by Goran [12]. From Fig. 3c and Table 2, it can be found

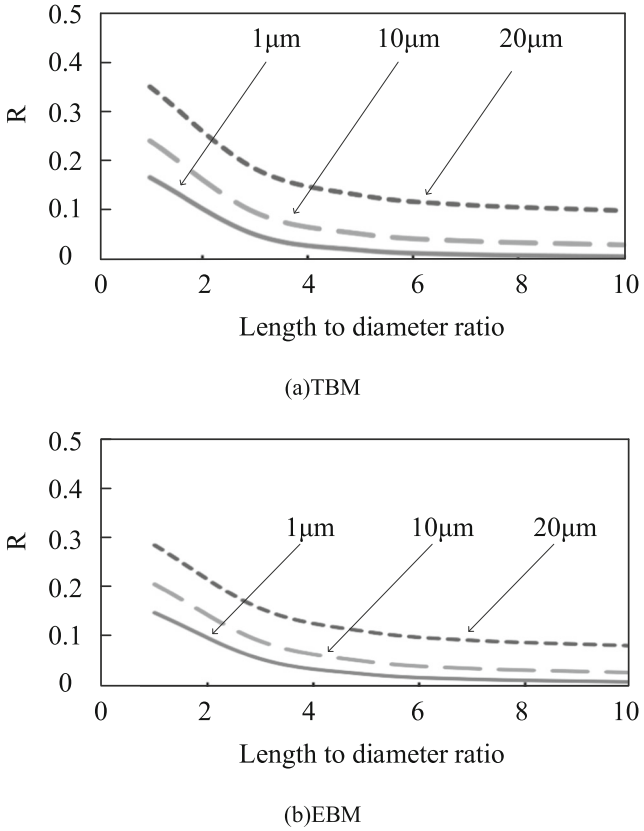

Fig. 4 Relative deflections of micro-end mill

that the maximum deflection of micro-end mill predicted by CT is about four times than that predicted by MCST and seven times than that predicted by SGET when the micro-end mill is taken to be a TBM. This is because the MCST considers the effect of rotation gradient tensor which can increase the stiffness of micro-end mill in addition to the strain tensor considered in classical theory. And relative to the MCST, the effect of stretch gradient tensor and dilatation gradient tensor are also taken into account in the SGET. When the micro-end mill is modeled as an EBM, the maximum deflection of micro-end mill is smaller than that when the micro-end mill is modeled as a TBM due to the shear effect being ignored in EBM. The influence of size effect on micro-end mill deflection using EBM is the same as when using TBM.

By contrasting Fig. 3a with Fig. 3c, the phenomenon can be found that the difference among deflections observed by different theories diminishes with the increase of tool diameter. For example, as shown in Table 2, when the tool diameter is equal to 20 μm, the maximum deflection predicted by the CT is only about 1.2 times than that predicted by the MCST and only 1.5 times than that predicted by the SGET when the micro-end mill is taken to be a TBM. It follows that the size effect is significant only when the tool diameter is comparable with the material length parameter.

In order to research the effect of length-to-diameter ratio of tool part on the deflection in detail, the deflections of micro-end mills with different length-to-diameter ratios and different tool diameters are obtained, and the relationships between the relative deflections (R) and the length-to-diameter ratios of tool part are shown in Fig. 4. R denotes the ratio of maximum deflections of micro-end mill obtained by SGET and that obtained by CT. It can be found from Fig. 4a that R decreases gradually with the increase of the length-to-diameter ratio when the micro-end mill is modeled as a TBM. And the phenomenon also appears when the micro-end mill is modeled as an EBM. It can be concluded that with the increase of the length-to-diameter ratio, the size effect becomes more obvious. With the increase of the length-to-diameter ratio, the proportion of tool part in the micro-end mill increases. As a consequence, the influence of size effect on deflections is more obvious with the increase in the length-to-diameter ratio. It also can be found that R increases with the increase of tool diameter, that is, the influence of size effect on deflections becomes more obvious with the decrease of the tool diameter.

3.2 Vibration of micro-end mill

The modal characteristics of micro-end mill influence the stability of micro-milling. The research on modal characteristics contributes in the selection of the machining parameters reasonably to obtain the required surface quality. The natural frequency of micro-end mill can be obtained by $\omega = (\mathbf{K}/\mathbf{M})^{1/2}$.

In order to research the influence of size effect on modal characteristics of micro-end mill, the first three natural frequencies and the corresponding mode shapes are calculated, as shown in Table 3 and Fig. 5. The geometric properties of micro-end mill selected in this research are shown in Table 1 except tool diameter and tool length.

From Table 3, it can be found that the natural frequencies predicted by SGET and MCST are larger than that predicted by CT when the tool diameter is less than 10 μm. This means that the micro-end mill stiffness increases when the size effect is considered. It also can be found that the size effect becomes obvious with the decrease of tool diameter and the increase of length-to-diameter ratio of the tool. This is because the ratio of tool part to the micro-end mill increases when the length-to-diameter ratio of the tool increases. Although the size effect has little effect on the natural frequency of the micro-milling tool, it has a great influence on the mode shapes, as shown in Fig. 5. Figure 5 shows the first three-

Table 1 Geometric properties of micro-end mill

Tool		Shank		Total length L (mm)
Diameter d_t (mm)	Length L_d (mm)	Diameter d_t (mm)	Length L_d (mm)	
0.001, 0.01, 0.02	0.01, 0.1	4	20	30

order mode shapes of micro-end mill in different cases. The special shape of the micro-end mill with thick shank and thin tool resulted in a large change in the mode shape, unlike the conventional uniform cantilever beam. When the size effect is considered, the vibration amplitude of the tool part decreases obviously. And the size effect phenomenon is more obvious with the increase of the length-to-diameter ratio.

In an actual micro-milling process, the micro-milling force changes with time due to the micro-milling system vibration, tool runout, and so on. To obtain the dynamic response of micro-end mill, Newmark scheme is utilized [33]. The condensed equation of the time-marching scheme for this case takes the form

$$\left(a_3[M]_{s+1}+[K]_{s+1}\right)\{u\}_{s+1} = \left(a_3\{u\}_s + a_4\{\dot{u}\}_s + a_5\{\ddot{u}\}_s\right)[M]_{s+1} + \{F\}_{s+1} \quad (12)$$

where

$$a_3 = \frac{1}{\beta(\Delta t)^2}, a_4 = a_3\Delta t, a_5 = \frac{1}{2\beta}-1, a_6 = \frac{\alpha}{\beta\Delta t}, \quad (13)$$

$$a_7 = \frac{\alpha}{\beta}-1, a_8 = \left(\frac{\alpha}{2\beta}-1\right)\Delta t$$

At the end of each time step, the new velocity vector and acceleration vector are computed using

$$\ddot{u}_{s+1} = a_3(u_{s+1}-u_s)-a_4\dot{u}_s-a_5\ddot{u}_s \quad (14)$$

$$\dot{u}_{s+1} = \dot{u}_s + a_2\ddot{u}_s + a_1\ddot{u}_{s+1} \quad (15)$$

where

$$a_1 = \alpha\Delta t,\ \ a_2 = (1-\alpha)\Delta t \quad (16)$$

In order to research the influence of size effect on dynamic response of micro-end mill, a harmonic force $F = F_0\sin(2\pi\omega t)$ is applied at the tool tip while the initial state of micro-end mill is at rest. Without loss of generality, the amplitude of the force $F_0 = 0.5$ N and the frequency $\omega = 500$ Hz. Figure 6 shows the response of tool tip of micro-end mill with different tool diameters under the same micro-milling force.

From Fig. 6, it can be seen that the maximum amplitude predicted by SGET is less than that predicted by MCST, and they are both less than that predicted by CT when $d_t = 10$ μm and $L_t = 10$ μm. It can be concluded that the stiffness of micro-end mill predicted by SGET is greater than that predicted by MCST, and they are both greater than that predicted by CT on account of the size effect. With the increase of tool diameter, all of the amplitudes of the micro-end mill predicted by the SGET, MCST, and CT decrease, and gradually have the tendency to be same. This is because the stiffness of the tool part of micro-end mill increases with the increase of tool diameter, to which the size effect is closely related. It can be found that the size effect can be neglected, and the SGET and MCST can be replaced by CT to predict the response of micro-end mill when the tool diameter is larger than 20 μm.

3.3 Experiments

Hammer modal experiment is the main method to measure modal parameters of traditional end mill, however, since the accelerometer sensor and its measuring cables used in the traditional modal test will generate additional mass and stiffness, which in turn changes the dynamic behavior of micro-end mill, this method is not suitable for measuring modal parameters of micro-end mill [34]. In order to overcome the shortcoming of traditional hammer modal test, non-contact measurement method is used in this test, in which the response

Table 2 Maximum deflection of micro-end mill (μm)

	TBM-SGET	TBM-MCST	TBM-CT	EBM-SGET	EBM-MCST	EBM-CT
$d_t = 20, L_t = 10$	5.156	7.048	8.119	4.171	7.013	7.627
$d_t = 10, L_t = 10$	8.645	16.814	31.821	6.130	15.317	30.520
$d_t = 1, L_t = 10$	158.315	5950	145,400	93.500	950	145,350

Table 3 Natural frequencies of micro-end mill (TBM) (Hz)

Mode	$d_t = 20$ μm and $L_t = 10$ μm			$d_t = 10$ μm and $L_t = 10$ μm			$d_t = 1$ μm and $L_t = 10$ μm		
	SGET	MCST	CT	SGET	MCST	CT	SGET	MCST	CT
1st	6447	6447	6447	6452	6452	6452	6457	6457	6457
2nd	34,791	34,790	34,790	34,831	34,829	34,828	34,866	34,864	34,864
3rd	79,498	79,494	79,493	79,644	79,638	79,636	79,775	79,769	79,767

of tool tip of micro-end mill is measured with laser displacement sensor instead of acceleration sensor. The non-contact modal test setup is shown in Fig. 7, the micro-end mill manufactured by NS TOOL is fixed on the worktable, adjusting the suspended length of micro-end mill equals to 30 mm. Two kinds of micro-end mills with $d_t = 30$ μm and $L_t = 45$ μm and with $d_t = 10$ μm and $L_t = 10$ μm are selected in this test. In order to fix the shank part of micro-end mill, a fixture is designed and manufactured by 3D printing technology, as shown in Fig. 7c. The fixture consists of two identical cuboids at 25 mm in length and 10 mm in width. And in the middle of the two cuboids, there is a half hole with a diameter of 3.9 mm for clamping the micro-end mill. Knocking the shank part of micro-end mill with impact hammer (CL-YD-303) and recording the force signal with data acquisition system supported by the B&K Corporation. The vibration displacement of corresponding point under the hammering force are measured using laser displacement sensor (Keyence LK-G30). The impact hammer has a sensitivity of 4.29 pC/N, and the laser sensor has a resolution of 10 nm and minimum sample period of 20 μs. And then, the frequency response functions (FRF) of micro-end mill can be calculated by transforming the measured vibration displacement and impulsed load from time domain to frequency domain using fast Fourier transform.

The measured vibration displacement, impulsed load, and FRF are shown in Figs. 8 and 9. In order to guarantee the accuracy of experimental results, the average of ten experiment results is taken as the final result to avoid the influence of other factors. The first-order natural frequency of micro-end mill which equal to 6213 Hz for $d_t = 10$ μm and $L_t = 10$ μm and 6237 Hz for $d_t = 30$ μm and $L_t = 45$ μm are obtained. The relative error between the experiment results and the theoretical results calculated

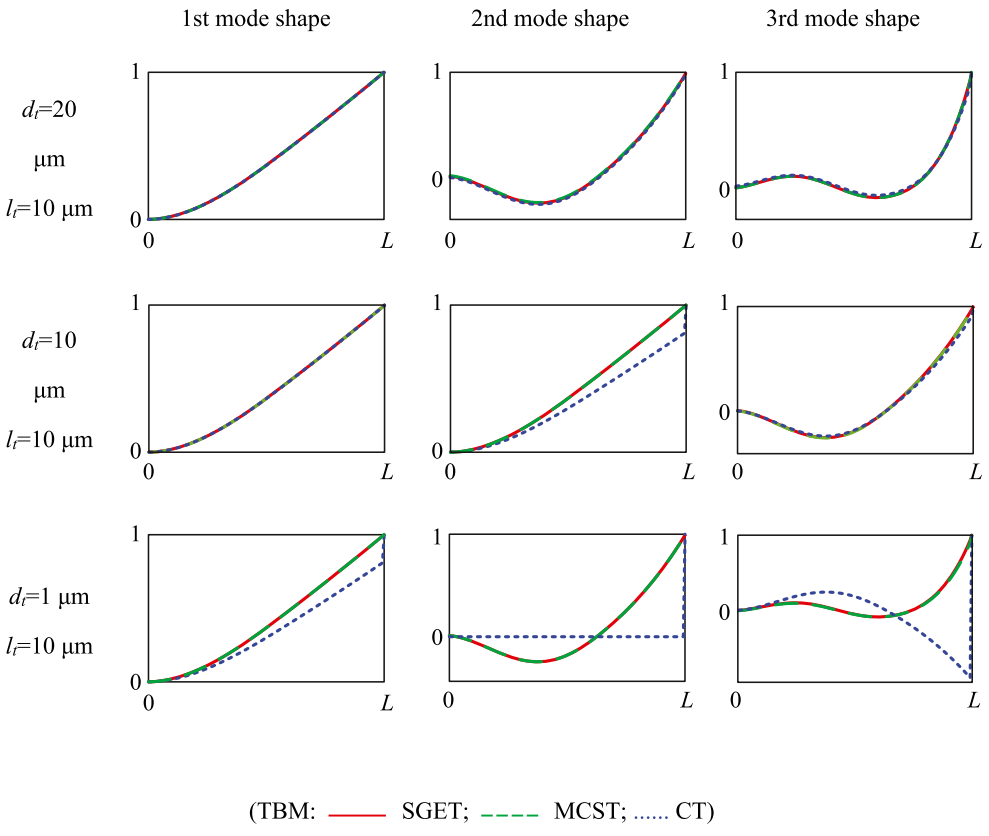

Fig. 5 Mode shapes of micro-end mill

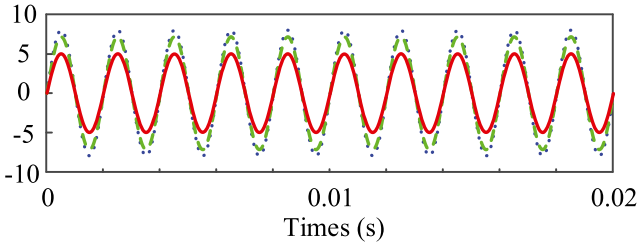

(a) d_t=20 μm, l_t=10 μm

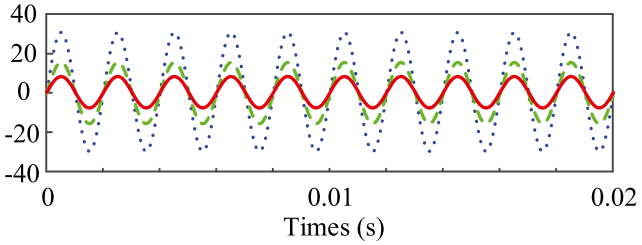

(b) d_t=10 μm, l_t=10 μm

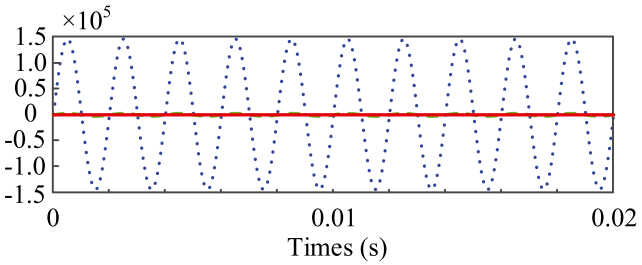

(c) d_t=1 μm, l_t=10 μm

(TBM: —— SGET; - - - MCST; ..... CT)

Fig. 6 Dynamic responses of micro-end mill under harmonic force

based on the method presented in this paper can be calculated by Eq. (17).

$$e = \frac{R_{\text{theoretical}} - R_{\text{experiment}}}{R_{\text{experiment}}} \times 100\% \tag{17}$$

Due to the clamping error, the precision error of equipment, the accuracy of measurement point, and excitation point in experiment, the results of micro-end mill obtained by the tests are less than the theoretical results. However, the relative error is 3.8% for $d_t = 10$ μm and $L_t = 10$ μm and 3.4% for $d_t = 30$ μm and $L_t = 45$ μm only.

Because the spot diameter of the laser displacement sensor (Keyence LK-G30) is about 30 μm, when the tool diameter of micro-end mill less than 30 μm, the laser emitted from the laser displacement sensor cannot be fully irradiated to the tool tip, resulting in inaccurate measurement position and measurement results. In order to measure the tool tip dynamic response of micro-end mill with tool diameter less than 30 μm under excitation force, the copper foil with 0.1 μm thickness is attached to the tool tip, as shown in Fig. 10. Due to the copper foil being thin and light, the influence of gold foil on tool tip dynamic response can be negligible. The micro-end mill is knocked with an impact hammer (CL-YD-303), and the vibration displacement of tool tip is measured with a laser displacement sensor (Keyence LK-G30). The experimental vibration displacements and theoretical vibration displacements of tool tip are shown in Fig. 11. It can be found that the tool tip dynamic response obtained by the presented method is in good agreement with the experimental results. Because the damping effect is neglected in the method proposed in this paper, the vibration of tool tip is not as attenuated as the experimental result.

In micro-milling process, surface roughness is closely related to the vibration of micro-end mill. The surface roughness can be simulated using cutting edge trajectory method [35].

$$\begin{cases} x(t) = f \cdot t + R\sin\varphi + x_r(t) + x_d(t) \\ y(t) = R\cos\varphi + y_r(t) + y_d(t) \end{cases} \tag{18}$$

where f is the feed speed, R represents the tool radius of micro-end mill, (x_r, y_r) denotes the deviations of cutting edge caused by the micro-end mill runout while (x_d, y_d) denotes the vibration of micro-end mill.

Therefore, cutting experiments are carried out to clarify the influence of the size effect on micro-end mill vibration. The experiments are performed on a micro-milling machine (Kern Micro 2522) with a spindle that can rotate up to 50,000 rpm and with a resolution of 0.1 μm. In the experiments, two micro-end mill with a tool diameter of 10 μm and a tool diameter of 30 μm are selected, and the material of micro-end mills are tungsten carbide. The material of workpiece with length of 100 mm, width of 50 mm, and height of 50 mm is aluminum alloy 7075. As shown in Fig. 12, the micro-end mill is installed on the spindle, adjusting the overhang length equal to 30 mm, while the workpiece is fixed on the fixture. The side- and up-milling methods are utilized in this experiment. Before the micro-milling experiments, the workpiece is machined through an end mill with a tool diameter of 1 mm to ensure the smoothness and levelness of the surface. The milling conditions are as follows: the spindle speed is 20,000 rpm, the radial cutting depth is 6 μm, the axial cutting depth is 10 μm, the feed speed is 2 mm/min, and the milling length is 2 mm. In order to ensure the accuracy of the experimental results, the experiment is carried out ten times for each micro-end mill.

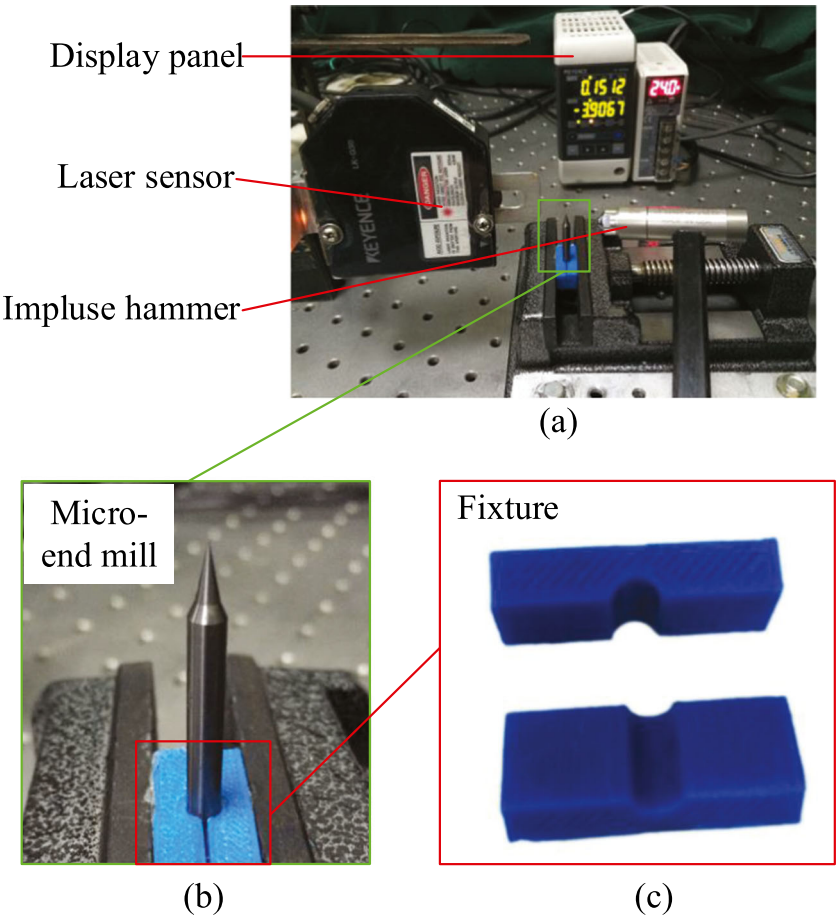

Fig. 7 Experimental setup for modal test

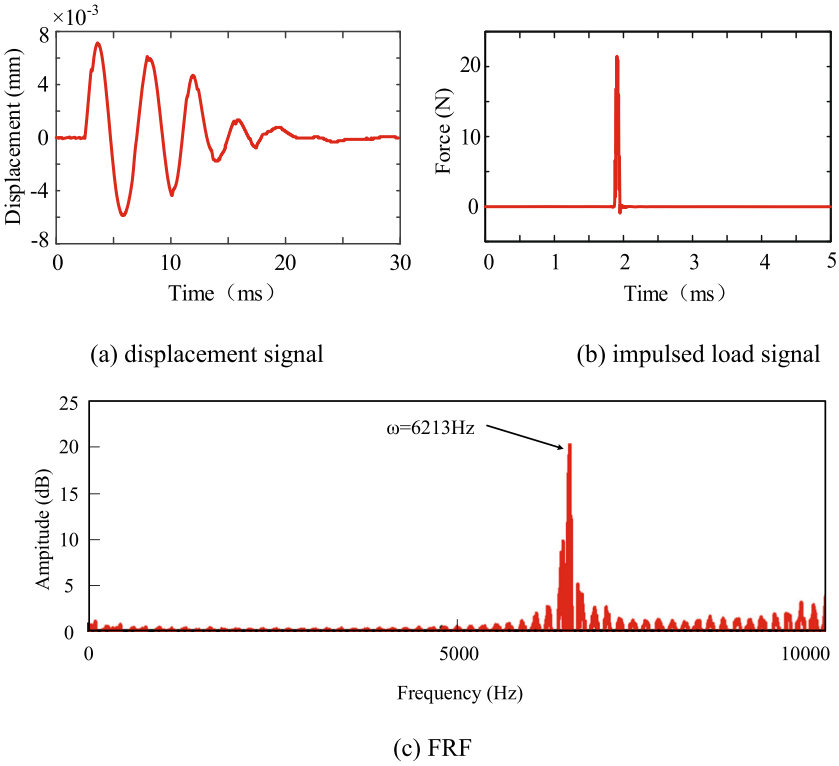

Fig. 8 Modal test results of micro-end mill with $d_t = 10$ μm and $L_t = 10$ μm

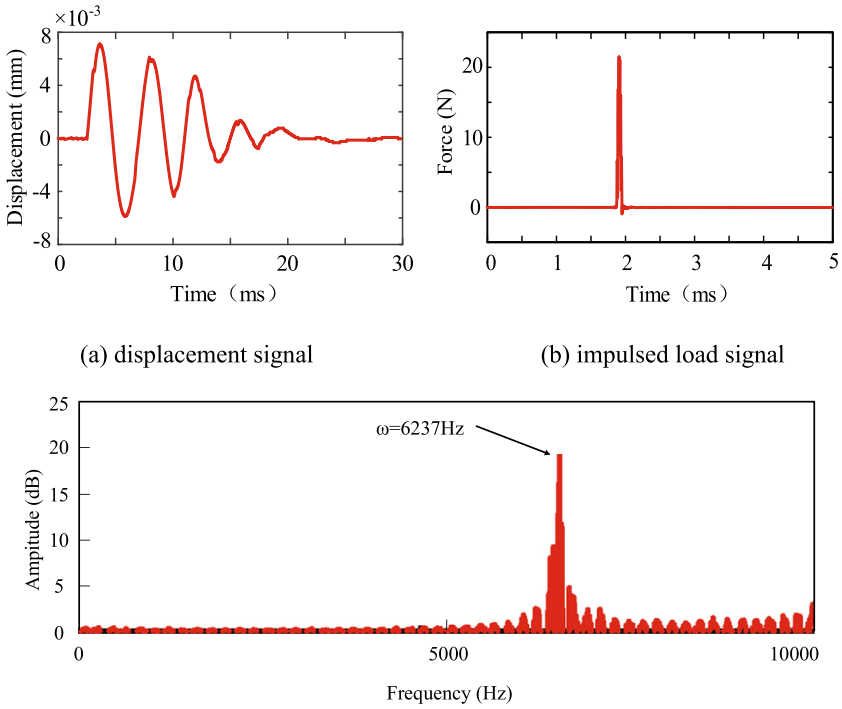

Fig. 9 Modal test results of micro-end mill with $d_t = 30$ μm and $L_t = 45$ μm

Figure 13a, b shows the surface roughness obtained with a micro-end mill having a diameter of 10 and 30 μm. From Fig. 13a, it can be found that the surface roughness simulated considering the size effect is similar to that simulated without considering the size effect, and they are slightly smaller than the experimentally measured surface roughness. This is because the simulation does not take into account the influence of other factors such as machine vibration. However, it can be clearly found from Fig. 13b that the simulated surface roughness is slightly greater than the experimentally measured surface roughness when the size effect of micro-end mill is neglected. When the size effect of micro-end mill is considered, the simulated surface roughness is slightly smaller than the experimentally measured surface roughness. And it can be found that compared with the simulation surface

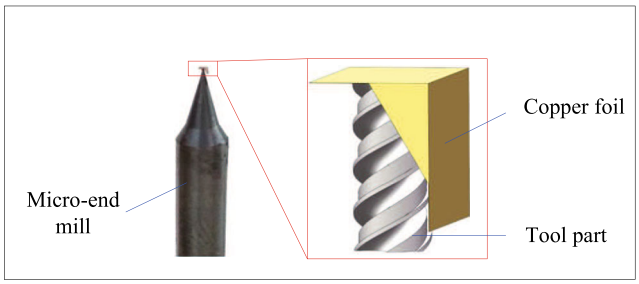

Fig. 10 Experimental setup for tool-tip response

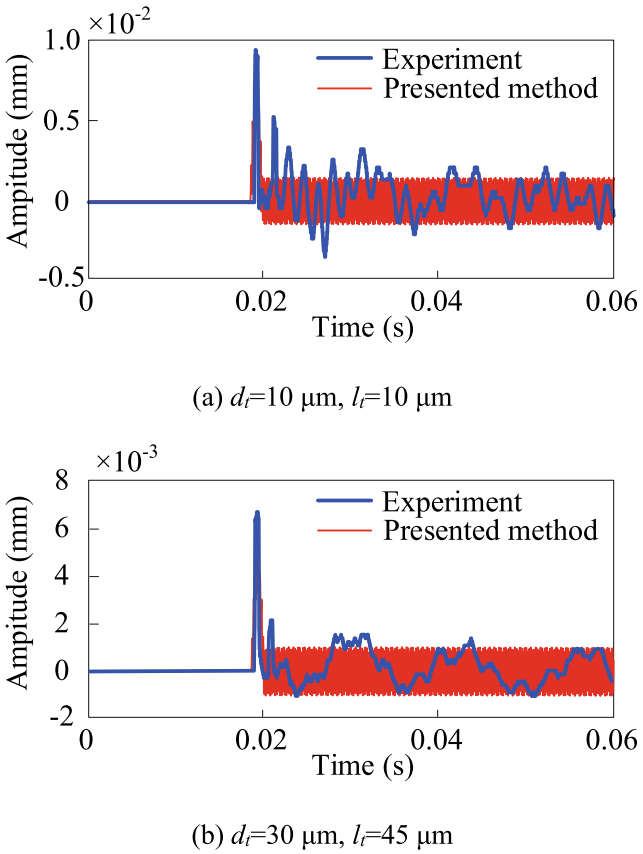

Fig. 11 Vibration displacements of tool tip

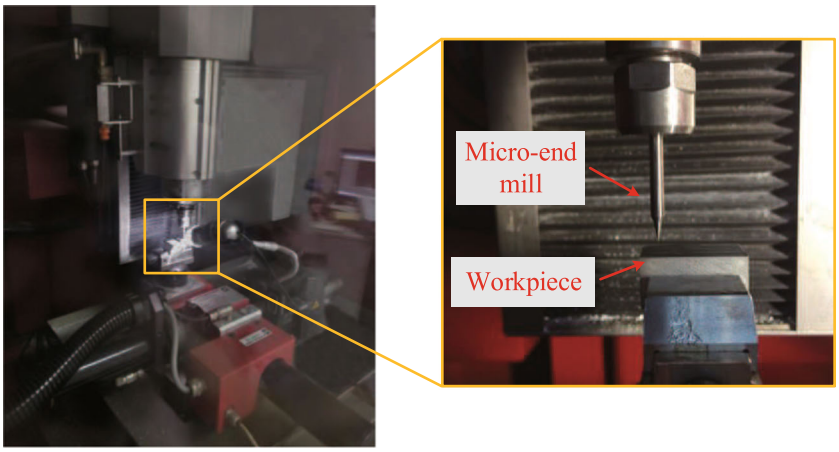

Fig. 12 Experimental setup for micro-milling

roughness without considering the size effect, the simulation surface roughness considering the size effect are more consistent with the experimentally measured surface roughness. It can be concluded that when the diameter of the tool part of micro-end mill is small, the size effect is obvious, and the size effect can increase the stiffness of micro-end mill and reduce the vibration amplitude of micro-end mill in machining process.

4 Conclusions

Based on the strain gradient elasticity theory and Hamilton's principle, a novel micro-end mill model is developed. In the presented model, in addition to traditional material constants, three material length parameters (l_0, l_1, l_2) which can predict the size effect are included. Considering shear deformation and micro-milling conditions, the micro-end mill is modeled as a cantilever Timoshenko beam. By using finite element method and experimental verification, the following conclusions can be obtained from the present work.

(i) Size effect can improve the stiffness of micro-end mill due to the rotation gradient tensor, stretch gradient tensor, and dilatation gradient tensor which are considered in the strain gradient elasticity theory.
(ii) The static deflection and dynamic response of tool tip decrease when the size effect is considered. Size effect is obvious only when the tool diameter is comparable with the material length parameters.
(iii) Due to the unique structure of thick shank and thin tool, the static bending deflections and mode shapes of micro-end mill vary greatly at the tool part. Although the size effect has little influence on the natural frequency, it has a great influence on the mode shapes.
(iv) The natural frequency and dynamic response obtained by the presented method are in good agreement with experimental results.

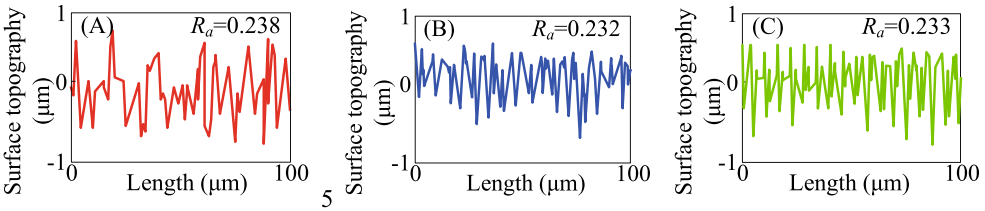

(a) surface roughness obtained using micro-end mill with d_t=30 μm

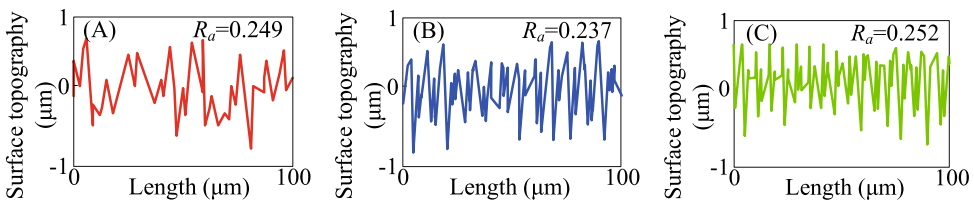

(b) surface roughness obtained using micro-end mill with d_t=10 μm

Fig. 13 Surface roughness obtained through experiment and numerical prediction. **a** Experimental surface roughness. **b** Surface roughness predicted based on the proposed method. **c** Surface roughness predicted based on the traditional method

Funding information The authors are grateful to the financial supports of the National Natural Science Foundation of China (no. 51875320), Young Scholars Program of Shandong University (no. 2015WLJH31), the United Fund of Ministry of Education for Equipment Pre-research (no. 6141A02022116), and the Key Research and Development Plan of Shandong Province (no. 2018GGX103007).

Compliance with ethical standards

Conflict of interest The authors declare that they have no conflict of interest.

Appendix 1

$$\varepsilon_{ij} = \frac{1}{2}\left(u_{i,j} + u_{j,i}\right) \tag{19}$$

$$\gamma_i = \varepsilon_{mm,i} \tag{20}$$

$$\eta^{(1)}_{ijk} = \frac{1}{3}\left(\varepsilon_{jk,i} + \varepsilon_{ki,j} + \varepsilon_{ij,k}\right) - \frac{1}{15}\delta_{ij}\left(\varepsilon_{mm,k} + 2\varepsilon_{mk,m}\right) - \frac{1}{15}\left[\delta_{jk}\left(\varepsilon_{mm,i} + 2\varepsilon_{mi,m}\right) + \delta_{ki}\left(\varepsilon_{mm,j} + 2\varepsilon_{mj,m}\right)\right] \tag{21}$$

$$\chi^{s}_{ij} = \frac{1}{2}\left(e_{ipq}\varepsilon_{qj,p} + e_{jpq}\varepsilon_{qi,p}\right) \tag{22}$$

$$\sigma_{ij} = k\delta_{ij}\varepsilon_{mm} + 2\mu\varepsilon'_{ij}, \varepsilon'_{ij} = \varepsilon_{ij} - \frac{1}{3}\varepsilon_{mm}\delta_{ij} \tag{23}$$

$$p_i = 2\mu l_0^2\gamma_i, \tau^{(1)}_{ijk} = 2\mu l_1^2\eta^{(1)}_{ijk}, m^{s}_{ij} = 2\mu l_2^2\chi^{s}_{ij} \tag{24}$$

where u_i is the displacement vector, δ_{ij} is the knocker tensor, e_{ijk} is the alternating tensor, k and μ are the bulk modulus and shear modulus, respectively. l_0, l_1, and l_2 are the material length-scale parameters.

Appendix 2

$$u_1(x,y,z,t) = -z\left(\frac{\partial w(x,t)}{\partial x} - \beta(x,t)\right), u_2(x,y,z,t) = 0, u_3(x,y,z,t) = w(x,t) \tag{25}$$

where u_1, u_2, and u_3 denote the three components of displacement vector in the x, y, and z directions, respectively. z denotes the distance from the centerline.

$$\varepsilon_{xx} = -z\left(\frac{\partial^2 w}{\partial x^2} - \frac{\partial\beta}{\partial x}\right), \varepsilon_{xz} = \frac{1}{2}\beta, \varepsilon_{yy} = \varepsilon_{zz} = \varepsilon_{xy} = \varepsilon_{yz} = 0 \tag{26}$$

$$\gamma_x = -z\left(\frac{\partial^3 w}{\partial x^3} - \frac{\partial^2\beta}{\partial x^2}\right), \gamma_y = 0, \gamma_z = -\frac{\partial^2 w}{\partial x^2} + \frac{\partial\beta}{\partial x} \tag{27}$$

$$\eta^{(1)}_{xxx} = -\frac{2}{5}z\left(\frac{\partial^3 w}{\partial x^3} - \frac{\partial^2\beta}{\partial x^2}\right), \eta^{(1)}_{xxz} = -\frac{4}{15}\left(\frac{\partial^2 w}{\partial x^2} - 2\frac{\partial\beta}{\partial x}\right),$$
$$\eta^{(1)}_{xyy} = \frac{1}{5}z\left(\frac{\partial^3 w}{\partial x^3} - \frac{\partial^2\beta}{\partial x^2}\right)$$
$$\eta^{(1)}_{xzx} = -\frac{4}{15}\left(\frac{\partial^2 w}{\partial x^2} - 2\frac{\partial\beta}{\partial x}\right), \eta^{(1)}_{xzz} = \frac{1}{5}z\left(\frac{\partial^3 w}{\partial x^3} - \frac{\partial^2\beta}{\partial x^2}\right),$$
$$\eta^{(1)}_{yxy} = \frac{1}{5}z\left(\frac{\partial^3 w}{\partial x^3} - \frac{\partial^2\beta}{\partial x^2}\right)$$
$$\eta^{(1)}_{yyx} = \frac{1}{5}z\left(\frac{\partial^3 w}{\partial x^3} - \frac{\partial^2\beta}{\partial x^2}\right), \eta^{(1)}_{yyz} = \frac{1}{15}\left(\frac{\partial^2 w}{\partial x^2} - 2\frac{\partial\beta}{\partial x}\right),$$
$$\eta^{(1)}_{yzy} = \frac{1}{15}\left(\frac{\partial^2 w}{\partial x^2} - 2\frac{\partial\beta}{\partial x}\right) \tag{28}$$
$$\eta^{(1)}_{zxx} = -\frac{4}{15}\left(\frac{\partial^2 w}{\partial x^2} - 2\frac{\partial\beta}{\partial x}\right), \eta^{(1)}_{zxz} = \frac{1}{5}z\left(\frac{\partial^3 w}{\partial x^3} - \frac{\partial^2\beta}{\partial x^2}\right),$$
$$\eta^{(1)}_{zyy} = \frac{1}{15}\left(\frac{\partial^2 w}{\partial x^2} - 2\frac{\partial\beta}{\partial x}\right)$$
$$\eta^{(1)}_{zzx} = \frac{1}{5}z\left(\frac{\partial^3 w}{\partial x^3} - \frac{\partial^2\beta}{\partial x^2}\right), \eta^{(1)}_{zzz} = \frac{1}{5}\left(\frac{\partial^2 w}{\partial x^2} - 2\frac{\partial\beta}{\partial x}\right)$$

$$\eta^{(1)}_{xxy} = \eta^{(1)}_{xyx} = \eta^{(1)}_{xyz} = \eta^{(1)}_{xzy} = \eta^{(1)}_{yxx} = \eta^{(1)}_{yxz} = \eta^{(1)}_{yyy} = \eta^{(1)}_{yzx} = \eta^{(1)}_{yzz} = \eta^{(1)}_{zxy} = \eta^{(1)}_{zyx} = \eta^{(1)}_{zyz} = \eta^{(1)}_{zzy} = 0$$

$$\chi^{s}_{xy} = \chi^{s}_{yx} = \frac{1}{4}\left(-2\frac{\partial^2 w}{\partial x^2} + \frac{\partial\beta}{\partial x}\right), \chi^{s}_{xx} = \chi^{s}_{yy} = \chi^{s}_{zz} = \chi^{s}_{yz} = \chi^{s}_{zx} = 0 \tag{29}$$

$$\sigma_{xx} = -\left(k + \frac{4}{3}\mu\right)z\left(\frac{\partial^2 w}{\partial x^2} - \frac{\partial\beta}{\partial x}\right), \sigma_{yy} = -\left(k - \frac{2}{3}\mu\right)z\left(\frac{\partial^2 w}{\partial x^2} - \frac{\partial\beta}{\partial x}\right)$$
$$\sigma_{zz} = -\left(k - \frac{2}{3}\mu\right)z\left(\frac{\partial^2 w}{\partial x^2} - \frac{\partial\beta}{\partial x}\right), \sigma_{xz} = \mu\beta, \sigma_{xy} = \sigma_{yz} = 0 \tag{30}$$

$$p_x = -2\mu l_0^2 z\left(\frac{\partial^3 w}{\partial x^3} - \frac{\partial^2\beta}{\partial x^2}\right), p_y = 0, p_z = -2\mu l_0^2\left(\frac{\partial^2 w}{\partial x^2} - \frac{\partial\beta}{\partial x}\right) \tag{31}$$

$$\begin{aligned}
&\tau_{xxx}^{(1)}=-\frac{4}{5}\mu l_1^2 z\left(\frac{\partial^3 w}{\partial x^3}-\frac{\partial^2\beta}{\partial x^2}\right),\tau_{xxz}^{(1)}=-\frac{8}{15}\mu l_1^2\left(\frac{\partial^2 w}{\partial x^2}-2\frac{\partial\beta}{\partial x}\right),\tau_{xyy}^{(1)}=\frac{2}{5}\mu l_1^2 z\left(\frac{\partial^3 w}{\partial x^3}-\frac{\partial^2\beta}{\partial x^2}\right)\\
&\tau_{xzx}^{(1)}=-\frac{8}{15}\mu l_1^2\left(\frac{\partial^2 w}{\partial x^2}-2\frac{\partial\beta}{\partial x}\right),\tau_{xzz}^{(1)}=\frac{2}{5}\mu l_1^2 z\left(\frac{\partial^3 w}{\partial x^3}-\frac{\partial^2\beta}{\partial x^2}\right),\tau_{yxy}^{(1)}=\frac{2}{5}\mu l_1^2 z\left(\frac{\partial^3 w}{\partial x^3}-\frac{\partial^2\beta}{\partial x^2}\right)\\
&\tau_{yyx}^{(1)}=\frac{2}{5}\mu l_1^2 z\left(\frac{\partial^3 w}{\partial x^3}-\frac{\partial^2\beta}{\partial x^2}\right),\tau_{yyz}^{(1)}=\frac{2}{15}\mu l_1^2\left(\frac{\partial^2 w}{\partial x^2}-2\frac{\partial\beta}{\partial x}\right),\tau_{yzy}^{(1)}=\frac{2}{15}\mu l_1^2\left(\frac{\partial^2 w}{\partial x^2}-2\frac{\partial\beta}{\partial x}\right)\\
&\tau_{zxx}^{(1)}=-\frac{8}{5}\mu l_1^2\left(\frac{\partial^2 w}{\partial x^2}-2\frac{\partial\beta}{\partial x}\right),\tau_{zxz}^{(1)}=\frac{2}{5}\mu l_1^2 z\left(\frac{\partial^3 w}{\partial x^3}-\frac{\partial^2\beta}{\partial x^2}\right),\tau_{zyy}^{(1)}=\frac{2}{15}\mu l_1^2\left(\frac{\partial^2 w}{\partial x^2}-2\frac{\partial\beta}{\partial x}\right)\\
&\tau_{zzx}^{(1)}=\frac{2}{5}\mu l_1^2 z\left(\frac{\partial^3 w}{\partial x^3}-\frac{\partial^2\beta}{\partial x^2}\right),\tau_{zzz}^{(1)}=\frac{2}{5}\mu l_1^2\left(\frac{\partial^2 w}{\partial x^2}-2\frac{\partial\beta}{\partial x}\right)
\end{aligned}\tag{32}$$

$$m_{xy}^{s}=m_{yx}^{s}=2\mu l_2^2\chi_{xy}^{s}=\frac{1}{2}\mu l_2^2\left(-2\frac{\partial^2 w}{\partial x^2}+\frac{\partial\beta}{\partial x}\right)\tag{33}$$

$$\begin{aligned}
U&=\frac{1}{2}\iiint_{\Omega}\left(\sigma_{ij}\varepsilon_{ij}+p_i\gamma_i+\tau_{ijk}^{(1)}\eta_{ijk}^{(1)}+m_{ij}^{s}\chi_{ij}^{s}\right)\mathrm{d}V\\
&=\frac{1}{2}\iiint_{\Omega}\left(\begin{array}{l}\left(k+\frac{4}{3}\mu\right)z^2\left(\frac{\partial^2 w}{\partial x^2}-\frac{\partial\beta}{\partial x}\right)^2+\mu\beta^2+2\mu l_0^2 z^2\left(\frac{\partial^3 w}{\partial x^3}-\frac{\partial^2\beta}{\partial x^2}\right)^2+2\mu l_0^2\left(\frac{\partial^2 w}{\partial x^2}-\frac{\partial\beta}{\partial x}\right)^2\\+\frac{4}{5}\mu l_1^2 z^2\left(\frac{\partial^3 w}{\partial x^3}-\frac{\partial^2\beta}{\partial x^2}\right)^2+\frac{8}{15}\mu l_1^2\left(\frac{\partial^2 w}{\partial x^2}-2\frac{\partial\beta}{\partial x}\right)^2+\frac{1}{4}\mu l_2^2\left(-2\frac{\partial^2 w}{\partial x^2}+\frac{\partial\beta}{\partial x}\right)^2\end{array}\right)\mathrm{d}V\\
&=\frac{1}{2}\int_0^L\left(k_1\varphi''^2+k_2\varphi'^2+k_3\left(-w''+2\varphi'\right)^2+k_4\left(w''+\varphi'\right)^2+k_5\left(w'-\varphi\right)^2\right)\mathrm{d}x
\end{aligned}\tag{34}$$

Appendix 3

$$\begin{aligned}
Q_1&=-\left[(k_4+k_5)\frac{\mathrm{d}^2 w}{\mathrm{d}x^2}+(-2k_4+k_5)\frac{\mathrm{d}\varphi}{\mathrm{d}x}\right]_{x=x_a}=-M(x_a)\\
Q_2&=\left[(k_1+k_3)\varphi''-(-2k_4+k_5)w''-(EI+k_2+4k_4+k_5)\varphi'\right]_{x=x_a}\\
&=Q^{h}(x_a)\\
Q_3&=\left[(k_4+k_5)\frac{\mathrm{d}^3 w}{\mathrm{d}x^3}+(-2k_4+k_5)\frac{\mathrm{d}^2\varphi}{\mathrm{d}x^2}-k_6\left(\frac{\mathrm{d}w}{\mathrm{d}x}-\varphi\right)\right]_{x=x_a}=V(x_a)\\
Q_4&=-\left[(k_1+k_3)\frac{\mathrm{d}v_2}{\mathrm{d}x}\varphi''\right]_{x=x_a}=-M^{h}(x_a)\\
Q_5&=\left[(k_4+k_5)\frac{\mathrm{d}^2 w}{\mathrm{d}x^2}+(-2k_4+k_5)\frac{\mathrm{d}\varphi}{\mathrm{d}x}\right]_{x=x_b}=M(x_b)\\
Q_6&=-\left[(k_1+k_3)\varphi''-(-2k_4+k_5)w''-(EI+k_2+4k_4+k_5)\varphi'\right]_{x=x_b}\\
&=-Q^{h}(x_b)\\
Q_7&=-\left[(k_4+k_5)\frac{\mathrm{d}^3 w}{\mathrm{d}x^3}+(-2k_4+k_5)\frac{\mathrm{d}^2\varphi}{\mathrm{d}x^2}-k_6\left(\frac{\mathrm{d}w}{\mathrm{d}x}-\varphi\right)\right]_{x=x_b}\\
&=-V(x_b)\\
Q_8&=\left[(k_1+k_3)\frac{\mathrm{d}v_2}{\mathrm{d}x}\varphi''\right]_{x=x_b}=M^{h}(x_b)
\end{aligned}\tag{35}$$

References

1. Oliaei SNB, Karpat Y (2016) Influence of tool wear on machining forces and tool deflections during micro milling. Int J Adv Manuf Technol 84(9–12):1963–1980
2. Bang Y, Lee K, Oh S (2005) 5-axis micro milling machine for machining micro parts. Int J Adv Manuf Technol 25(9–10):888–894
3. Gao P, Liang Z, Wang X, Li S, Zhou T (2018) Effects of different chamfered cutting edges of micro end mill on cutting performance. Int J Adv Manuf Technol 96(1–4):1215–1224
4. Lu X, Wang F, Jia Z, Si L, Zhang C, Liang SY (2017) A modified analytical cutting force prediction model under the tool flank wear effect in micro-milling nickel-based superalloy. Int J Adv Manuf Technol 91(9–12):3709–3716
5. Zhang X, Ehmann KF, Yu T, Wang W (2016) Cutting forces in micro-end-milling processes. Int J Mach Tools Manuf 107:21–40
6. Huo D, Chen W, Teng X, Lin C, Yang K (2017) Modeling the influence of tool deflection on cutting force and surface generation in micro-milling. Micromachines 8(6):188
7. Mustapha KB, Zhong ZW (2013) A new modeling approach for the dynamics of a micro end mill in high-speed micro-cutting. J Vib Control 19(6):901–923
8. Filiz S, Ozdoganlar OB (2011) A three-dimensional model for the dynamics of micro-endmills including bending, torsional and axial vibrations. Precis Eng 35(1):24–37

9. Yılmaz EE, Budak E, Özgüven N (2016) Modeling and measurement of micro end mill dynamics using inverse stability approach. Procedia CIRP 46:242–245
10. Rodriguez P, Labarga JE (2015) Tool deflection model for micromilling processes. Int J Adv Manuf Technol 76(1–4):199–207
11. Duncan GS, Schmitz TL (2005) An improved RCSA model for tool point frequency response prediction. Precis Eng 33(1):26–36
12. Mijušković G, Krajnik P, Kopač J (2015) Analysis of tool deflection in micro milling of graphite electrodes. Int J Adv Manuf Technol 76(1–4):209–217
13. Li P, Oosterling JAJ, Hoogstrate AM, Langen HH, Schmidt RHM (2011) Design of micro square endmills for hard milling applications. Int J Adv Manuf Technol 57(9–12):859–870
14. Filiz S, Ozdoganlar OB (2008) Microendmill dynamics including the actual fluted geometry and setup errors—part I: model development and numerical solution. J Manuf Sci Eng 130(3):031119
15. Filiz S, Ozdoganlar OB (2008) Microendmill dynamics including the actual fluted geometry and setup errors—part II: model validation and application. J Manuf Sci Eng 130(3):031120
16. Jun MBG, Devor RE, Kapoor SG (2006) Investigation of the dynamics of microend milling—part II: model validation and interpretation. J Manuf Sci Eng 128(4):901–912
17. Kong S, Zhou S, Nie Z, Wang K (2009) Static and dynamic analysis of micro beams based on strain gradient elasticity theory. Int J Eng Sci 47(4):487–498
18. Liang B, Zhang L, Wang B, Zhou S (2015) A variational size-dependent model for electrostatically actuated NEMS incorporating nonlinearities and Casimir force. Phys E 71:21–30
19. Ataei H, Beni YT, Shojaeian M (2016) The effect of small scale and intermolecular forces on the pull-in instability and free vibration of functionally graded nano-switches. J Mech Sci Technol 30(4):1799–1816
20. Mindlin RD, Tiersten HF (1962) Effects of couple-stresses in linear elasticity. Arch Ration Mech Anal 11(1):415–448
21. Yang F, Chong ACM, Lam DCC, Tong P (2002) Couple stress based strain gradient elasticity theory for elasticity. Int J Solids Struct 39(10):2731–2743
22. Mindlin RD, Eshel NN (1968) On first strain-gradient theories in linear elasticity. Int J Solids Struct 4(1):109–124
23. Lam DCC, Yang F, Chong ACM, Wang J, Tong P (2003) Experiments and theory in strain gradient elasticity. J Mech Phys Solids 51(8):1477–1508
24. Song Q, Liu Z, Shi Z (2014) Chatter stability for micromilling processes with flat end mill. Int J Adv Manuf Technol 71(5–8):1159–1174
25. Chen CC, Liu NM, Chiang KT, Chen HL (2012) Experimental investigation of tool vibration and surface roughness in the precision end-milling process using the singular spectrum analysis. Int J Adv Manuf Technol 63(5–8):797–815
26. Singh KK, Singh R (2018) Chatter stability prediction in high-speed micromilling of Ti6Al4V via finite element based microend mill dynamics. Adv Manuf 6(1):95–106
27. Kahrobaiyan MH, Asghari M, Ahmadian MT (2014) A Timoshenko beam element based on the modified couple stress theory. Int J Mech Sci 79(75–83):75–83
28. Wang B, Zhao J, Zhou S (2009) A micro scale Timoshenko beam model based on strain gradient elasticity theory. Eur J Mech-A/Solids 29(4):591–599
29. Shi Y, Mahr F, Wagner UV, Uhlmann E (2013) Gyroscopic and mode interaction effects on micro-end mill dynamics and chatter stability. Int J Adv Manuf Technol 65(5–8):895–907
30. Reddy JN (1999) On the dynamic behaviour of the Timoshenko beam finite elements. Sadhana 24(3):175–198
31. Voyiadjis GZ, Almasri AH (2009) Variable material length scale associated with nanoindentation experiments. J Eng Mech 135(3):139–148
32. Song JR, Liu JY, Wei YG (2011) A kind of physics interpretations of material length scales. ICHMM:341–347
33. Lee AC, Hoang TD (2016) Coupled lateral and torsional vibrations of the micro-drilling spindle systems. Int J Adv Manuf Technol 87(5–8):2063–2079
34. Maekawa A, Noda M, Shintani M (2016) Experimental study on a noncontact method using laser displacement sensors to measure vibration stress in piping systems. Measurement 79:101–111
35. Yuan Y, Jing X, Ehmann KF, Zhang D (2018) Surface roughness modeling in micro end-milling. Int J Adv Manuf Technol 95(5–8):1655–1664